High loading BaTiO3 nanoparticles chemically bonded with fluorinated silicone rubber for largely enhanced dielectric properties of polymer nanocomposites

Fang-Yan Du, Rui-Chao Chen, Junjin Che, Wei-Di Xu, Xiu Liu, Yin-Tao Li, Yuan-Lin Zhou, Jinkai Yuan, Quan-Ping Zhang

High loading $BaTiO_3$ nanoparticles chemically bonded with fluorinated silicone rubber for largely enhanced dielectric properties of polymer nanocomposites

Fang-Yan Du [a#], Rui-Chao Chen [a#], Junjin Che [b], Wei-Di Xu [a], Xiu Liu [a], Yin-Tao Li [a], Yuan-Lin Zhou [a], Jinkai Yuan [b]*, Quan-Ping Zhang [a]*

[a] *State Key Laboratory of Environment-friendly Energy Materials, School of Materials Science and Engineering, Southwest University of Science and Technology, Mianyang 621010, China*
[b] *Centre de Recherche Paul Pascal, CNRS, University of Bordeaux, UMR5031, 33600 Pessac, France*

Abstract

Integrating high-loading dielectric nanoparticles into polar polymer matrices potentially can profit the intrinsic polarization of each phase and allow for greatly enhanced dielectric properties in polymer nanocomposites. It is however challenging to achieve desirable highly filled polar polymer composites because of the lack of efficient approaches to disperse nanoparticles and maintain interfacial compatibility. Here, we report a versatile route to fabricate highly filled barium titanate/fluorinated silicone rubber (BT/FSR) nanocomposites by ‘‘thiol-ene click’’ and isostatic pressing techniques. The loaded BT nanoparticles (from 82 wt.% to 90 wt.%) are chemically bonded with FSR in the nanocomposites. The existence of the polar group ($-CH_2CF_3$) of the polymer matrix does not affect the uniform dispersion of the nanoparticles and the good interfacial compatibility as well. 90 wt.% BT/FSR nanocomposite shows the highest dielectric constant of 57.8 at 10^3 Hz, while the loss tangent can be kept below 0.03. Besides, BT/FSR nanocomposites display the higher breakdown strength than BT/SR nanocomposites, respectively. This work offers a facile strategy towards superior dielectric properties of polymer nanocomposites.

Keywords: Dielectric constant; $BaTiO_3$ nanocomposites; Highly filled polymer

Corresponding authors: Jinkai Yuan; Quan-Ping Zhang
E-mails: jinkai.yuan@crpp.cnrs.fr; zhangqp@swust.edu.cn
F.Y. and R.C. contributed equally.

Introduction

Polymer dielectric materials are featured with various merits such as good processability, flexibility, light-weight, low cost, and high breakdown strength [1-6], which have been extensively applied to advanced electronic devices such as capacitor, actuator, sensor and electro-magnetic interference shielding [7-12]. However, most of polymers bear intrinsically low dielectric constant because of the low dipole moments of the chemical bonds in spite of other excellent dielectric properties. Ferroelectric polymers such as polyvinylidene fluoride (PVDF) and its copolymers enjoy a relatively high dielectric constant thanks to the high polarization of the C−F bonds and the spontaneous orientation of dipoles in the crystalline domains. However, their considerable dielectric loss is an unfavorable trait [13-17]. Therefore, developing polymer dielectric materials with excellent overall dielectric properties is of vital significance for their applications in the electronic and electrical industry.

The studies on blending polar polymers such as PVDF with dielectric nanoparticles such as $BaTiO_3$ (BT) have been conducted to enhance the dielectric constant of polymer nanocomposites and significant progress has been made [18-20]. This is due to the fact that the intrinsic polarizations of both dielectric nanoparticles and polar polymers can be explored at the same time. To take full advantage of their intrinsic polarizations, developing highly-filled polar polymer nanocomposites is one of the most effectively strategies that allows for largely enhanced dielectric constant. Unfortunately, several defects such as nonuniform dispersion of nanoparticles, incompatible interfaces, as well as voids tend to be formed in the highly-filled polar polymer nanocomposites [21-23]. Then, charge separation at the incompatible interfaces, intensified local electric field and leakage current easily occur in the polymer nanocomposites, which cause degraded dielectric properties, in particular the dielectric loss and breakdown strength [24-31]. To date, the optimum loading of nanoparticles in polar polymer nanocomposites for excellent overall dielectric properties has been achieved within a relatively low content. This is due to the fact

that relatively weak intermolecular forces such as hydrogen bond between polar polymers and nanoparticles fail to support sufficiently strong interface interaction in highly-filled polymer nanocomposites.

Constructing sufficient covalent bonds between polar polymer and nanoparticles is of great interest to avoid the formation of defects in highly-filled polymer nanocomposites. To date, ‘‘grafting to’’ and ‘‘grafting from’’ means have been used to chemically bond nanoparticles with polymers for strengthening the interfacial interactions [21, 32-39]. In our previous work, more than 88 wt.% BT nanoparticles are chemically bonded with a nonpolar silicone rubber (SR) via “thiol-ene click” technique [40]. The intrinsic polarizations of nanoparticles was extremely utilized, which gives rise to greatly improved dielectric properties in polymer nanocomposites. Numerous studies have shown that incorporating polar groups into the side and/or main chains of polymers also significantly promotes the dielectric constant of polymer nanocomposites [41-44]. However, highly-filled polar polymer nanocomposites ($>$ 80 wt%) are still to be explored. It makes use of intrinsic polarizations of both polar polymers and dielectric nanoparticles to an extreme. Then, dielectric constant, dielectric loss as well as breakdown strength can be compromised for excellent overall dielectric properties of polymer nanocomposites.

In this paper, a facile route is proposed to chemically bond high loading BT nanoparticles with polar polymer fluorinated silicone rubber for improving dielectric properties of polymer nanocomposites. First, a fluoropolymer (polysiloxane with trifluoropropyl groups in side chain) is synthesized via anionic ring opening polymerization. Second, BT nanoparticles are superficially modified to graft thiol group on their surfaces. Third, a powerful and versatile ‘‘thiol-ene click’’ technique is applied to chemically bond BT nanoparticles with FSR. Note that the 90 wt% BT/FSR nanocomposite shows the largest dielectric constant of 57.8 at 10^3 Hz ever reported for polymer-based composites with 0 dimensional BT nanoparticles. Meanwhile, its dielectric loss can be kept below 0.03. Besides, 88 wt.% and 82 wt.% BT/FSR nanocomposites have the higher breakdown strength than BT/SR counterparts,

respectively. This work paves the way to take extreme advantage of the intrinsic polarizations of polar polymer and dielectric nanoparticles to greatly improve the overall dielectric properties of polymer nanocomposites.

Results and discussion

Fabrication of highly-filled polar polymer nanocomposites

Fabricating the highly-filled polar polymer nanocomposites includes three steps, as depicted in **Figure 1**. **Step 1**: Two kinds of monomer 1, 3, 5, 7-tetravinyl-1, 3, 5, 7-tetramethylcyclotetrasiloxane (V_4) and 1, 3, 5-Trimethyl-1, 3, 5-tris(3, 3, 3-trifluoropropyl) cyclotrisiloxane (D_3F) with an volume ratio of 4: 6, the initiator tetramethylammonium hydroxide (TMAH) are mixed together. Then, a kind of fluorinated polysiloxane is obtained after triggering anionic ring opening polymerization [45]. **Step 2**: BT nanoparticles are first treated with hydrogen peroxide aqueous solution to form hydroxyl groups on the surface of the nanoparticles (BT-OH). Then BT nanoparticles are further modified with KH580 to achieve the sulfhydryl modification (BT-SH) [46]. **Step 3**: the BT-SH (82 wt.%, 84 wt.%, 86 wt.%, 88 wt.% and 90 wt.%), the fluorinated polysiloxane, a cross-linker 3, 6-Dioxa-1, 8-octanedithiol (DODT) and a radical initiator 2, 2-dimethoxy-2-phenylacetophenone (DMPA) are compounded together with toluene. Afterwards, conventional tableting technique is applied to initially fabricate the samples with a pressure of 1.5 MPa for 1 minute. Following that, an isostatic pressing technique is applied to further press the prefabricated samples with a greatly high pressure of 260 MPa for 10 minutes [40]. Finally, BT nanoparticles are chemically bonded with FSR in the samples when a typical “thiol-ene click” reaction is triggered at 80 °C. **Table 1** lists Shore D hardness of the highly-filled polymer nanocomposites. The hardness increases from 45 D to 58 D with increasing the BT nanoparticles. It indicates the highly filled silicone rubber nanocomposite displays almost ceramic-like rigidity rather rubber-like flexibility.

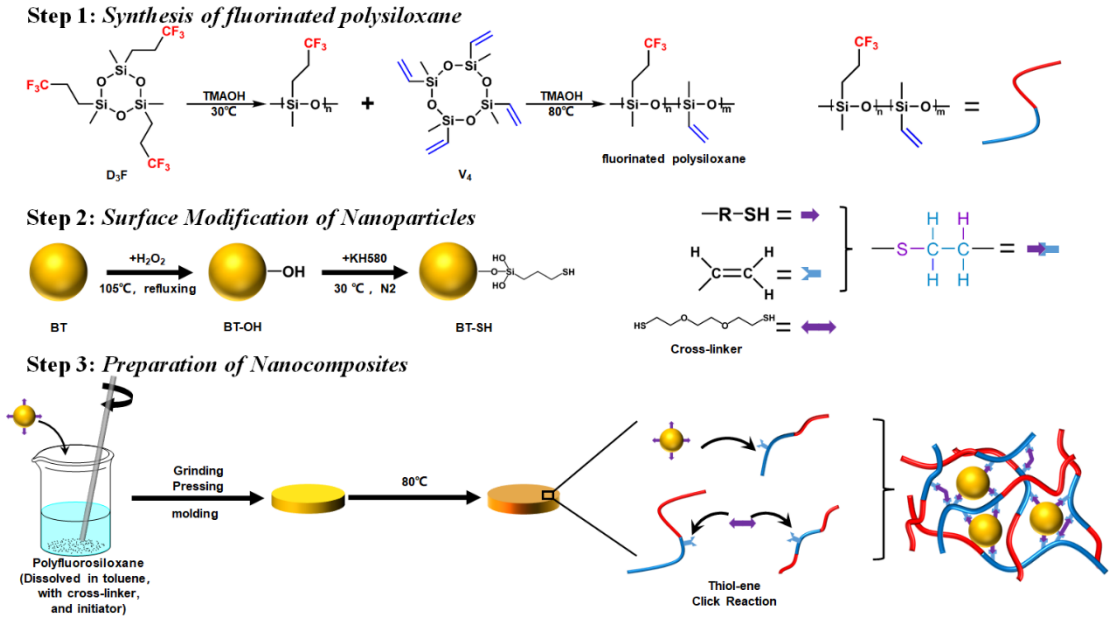

Figure 1. Schematic illustration for the fabrication route towards highly-filled polar polymer nanocomposites

Table 1. Shore D hardness of the highly-filled polymer nanocomposites

BT loading	**82 wt%**	**84 wt%**	**86 wt%**	**88 wt%**	**90 wt%**
Shore D	46	48	51	55	58

Chain structures of the prepared polysiloxanes are determined by FT-IR and 1H NMR techniques, respectively. As depicted in **Figure 2(a),** both the polysiloxanes display strong peaks at 1598.7 cm^{-1} for vinyl group. Furthermore, the fluorinated polysiloxane shows more characteristic peaks, including C-F band at 1210.6 cm^{-1}, C-C band of $-CH_2-CF_3$ at 901.1 cm^{-1}, C-C band of $-CH_2-CH_2-$ at 1315.7 cm^{-1}, and C-H band of $-CH_2-CH_2-$ at 1128.6 cm^{-1}. This is due to the fact that the fluorinated polysiloxane possesses the side chain of trifluoropropyl groups ($-CH_2CF_3$) while the polymethylvinylsiloxane without. As depicted in **Figure 2(b)**, the main H chemical shift peak appears at δ = 0.25 ppm, δ = 0.8 ppm, δ = 2.1 ppm, δ = 5.8 ppm and δ = 5.9 ppm, corresponding to the H chemical shifts of $Si-CH_3$(a), $Si-CH_2$-(b), $-CH_2-CF_3$(c), -CH= (d) and $=CH_2$ (e) respectively. The chemical shift integral area ratio of ***Peak b***, ***Peak* c** and ***Peak e*** is approximately 1:1:1.25. Therefore, the fluorinated polysiloxane is a typical block copolymer and its block ratio of ***m*** to ***n*** is 5:4.

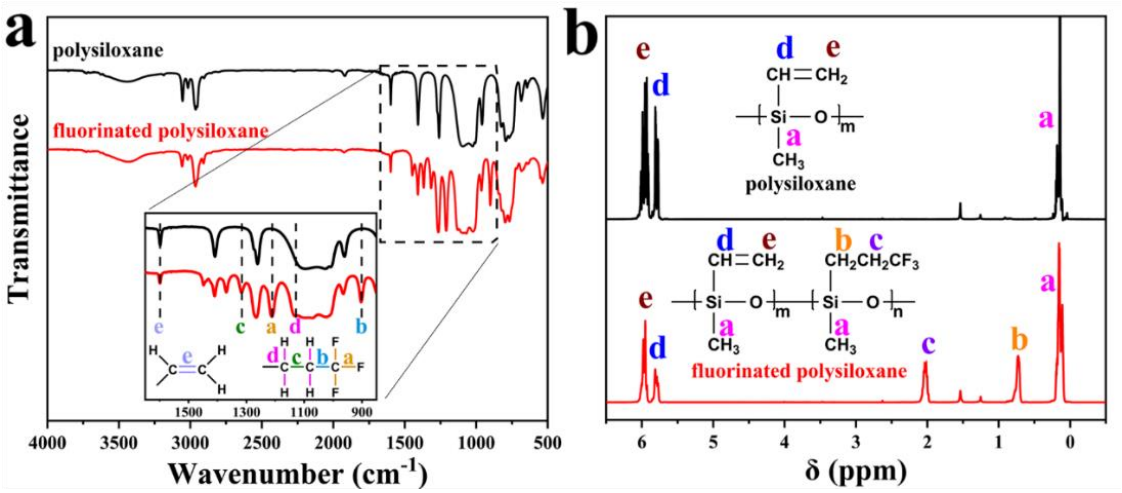

Figure 2. (a) FT-IR spectrum and (b) 1H NMR spectrum of the prepared polysiloxane and its fluoropolymer.

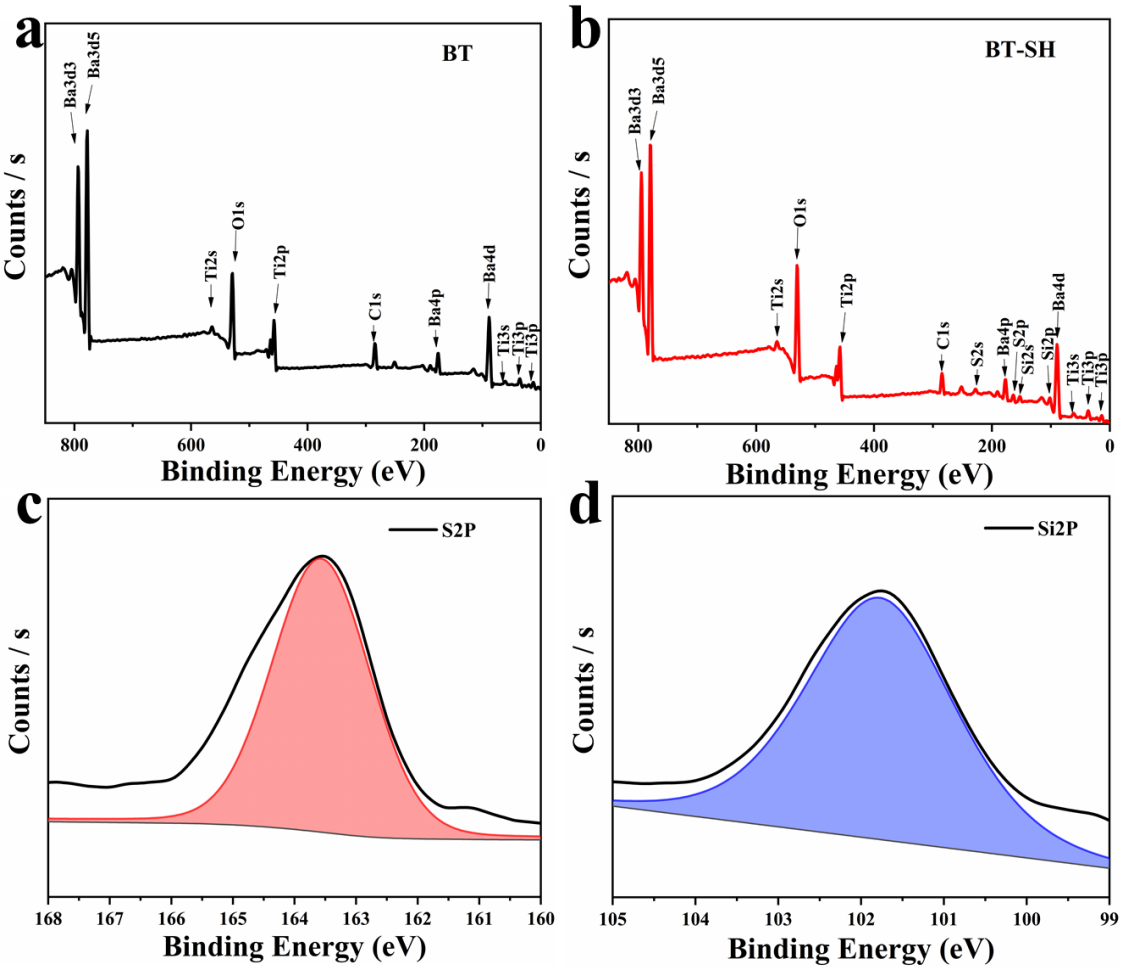

Figure 3. Wide-scan XPS spectrum of (A) neat BT and (B) BT-SH; (C) S2p and (D) Si2p spectrum of BT-SH.

Thiols (-SH) on the surface of BT nanoparticles are determined by XPS technique, as shown in **Figure 3**. The characteristic signals for silicon (Si2p at 101.75 eV) and sulphur (S2p at 163.55 eV) are clearly observed in the wide scan spectrum [46], as shown in **Figure 3(a)** and **Figure 3(b).** The signals of S and Si on the surfaces of BT-SH nanoparticles are further confirmed in **Figure 3(c)** and **Figure 3(d)**. To determine the grafting density of –SH on BT nanoparticles, TGA test is conducted, as shown in **Figure S1**. The results also indicate –SH is successfully grafted on the surfaces of BT nanoparticles and its grafting density is about 10.3 groups nm^{-2} according to thermal weight loss.

Morphologies of highly-filled polar polymer nanocomposites

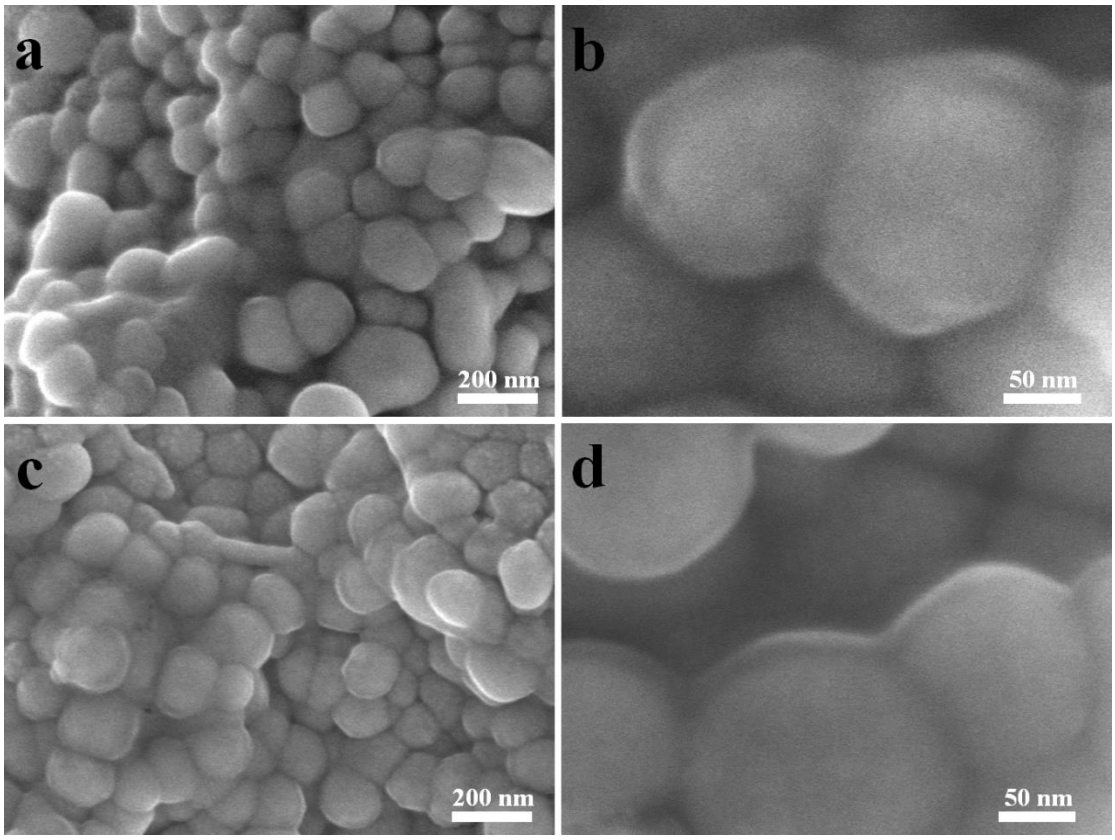

Figure 4. SEM images of BT/FSR (a, b) and BT/SR (c, d) nanocomposites with 88wt.% BT nanoparticles

Figure 4 displays the microstructure of highly-filled BT/FSR and BT/SR nanocomposites, in order to investigate the effect of incorporating polar groups into polymer matrix on the morphologies. **Figure 4 (a)** and **Figure 4(b)** show that BT

nanoparticles are coated uniformly meanwhile bonded with a thin SR layer in the BT/SR nanocomposite with 88 wt.% BT, which is completely consistent with our previous work [45]. This is because all the thiols on the surfaces of BT nanoparticles can react with the excess enes (-CH=CH_2) in the polymethylvinylsiloxane chains via the typical ‘‘thiol-ene click’’. It leads to the desirable uniform dispersion of BT nanoparticles and good interfacial compatibility in the highly filled polymer nanocomposites. Interestingly, the similar microstructure on the dispersion of BT nanoparticles and interfacial compatibility can also be seen in the BT/FSR nanocomposites with 88 wt.% BT nanoparticles, as shown in **Figure 4 (c)** and **(d)**. It indicates that although the amount of vinyl group in the polymer matrix is decreased after incorporating the polar group, it is sufficient to react with all the thiols on the surfaces of BT nanoparticles. Besides, the desirable morphologies can also be observed at 82 wt.%, 86 wt.% and 90 wt.% BT/FSR nanocomposite, as depicted in **Figure S2**. Fewer defects can be found in the nanocomposite with the lower BT loadings.

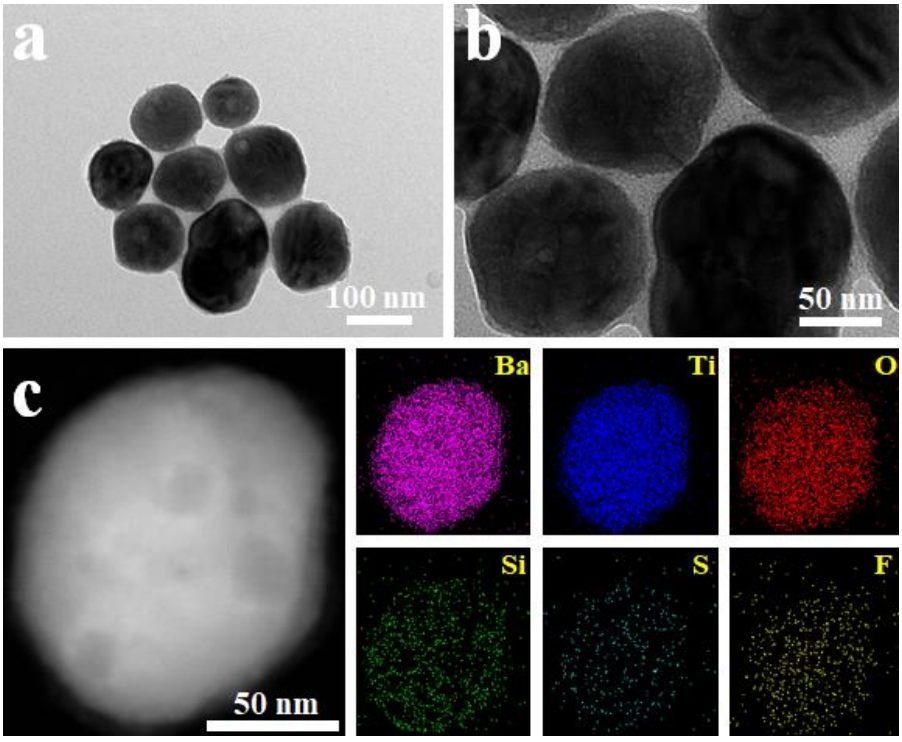

Figure 5. TEM results of 88 wt.% BT/FSR nanocomposites, (a, b) TEM images and (c) TEM-EDX mapping.

TEM techniques are performed to further determine the microstructure of BT/FSR nanocomposites, as shown in **Figure 5**. BT nanoparticles are tightly bonded with FSR matrix rather than directly connected with each other, as depicted in **Figure 5(a)** and **Figure 5(b)**. It implies that the fluorinated polysiloxane is anchored on the surface of BT nanoparticles with rich covalent bonds, leading to the desirable morphologies in spite of highly loaded BT nanoparticles. In addition, **Figure 5(c)** displays the mapping analysis of the nanocomposites. Uniform distribution of all the elements can be observed obviously. Among them, Ba, Ti and O mainly are mainly supplied by BT nanoparticles. S is from the thiol groups on the surface of BT nanoparticles and cross-linkers. Besides, F is supplied by the side chains in the fluorinated polysiloxane. The TEM results further indicate incorporating the fluorinated silicone rubber also leads to a series of desirable features such as uniform dispersion of nanofillers, good interfacial compatibility in highly-filled polar polymer nanocomposites.

Dielectric properties of highly-filled polymer nanocomposites

Figure 6(a) depicts the dielectric constants of neat polymers and its highly filled nanocomposites. Neat FSR displays higher dielectric constants in comparison with neat SR. The former shows a dielectric constant of 5.13 at 10^3 Hz, which is twice as much as that of the latter, as displayed in **Figure 6(c)**. This is due to much more dipoles existing in the polar polymer. Then, 88 wt.% BT/FSR nanocomposite shows higher dielectric constant than 88 wt.% BT/SR nanocomposite due to the additional polarization from the polar polymer matrix. It possesses a dielectric constant of 52.4 at 10^3 Hz, which is approximately 1.45 times higher than that of its counterpart. The results demonstrate that incorporating polar groups into polymer matrix dramatically promotes the dielectric constants of polymer nanocomposites. The similar frequency dependences of dielectric constant indirectly verify the similar morphologies in both the polymer nanocomposites. Besides, it can be observed that 90 wt.% BT/FSR nanocomposite displays the largest dielectric constant. The dielectric constant gradually decreases with the decreasing BT loading. 82 wt.% BT/FSR nanocomposite

still displays a higher dielectric constant than 88 wt.% BT/SR nanocomposite while its dielectric losses is obviously lower than that of the counterpart, which are very close to that of the neat polymer, as depicted in **Figure 6(b)** and **Figure 6(d)**. This is because more polymers contributes to filling into the voids between BT nanoparticles and then fewer defects of microstructures tend to be formed in the nanocomposites at the lower BT loading. The results indicate that enhanced dielectric constant meanwhile reduced dielectric loss of polymer nanocomposites can be achieved by chemically bonding fluorinated silicone rubber with high loading BT nanoparticles.

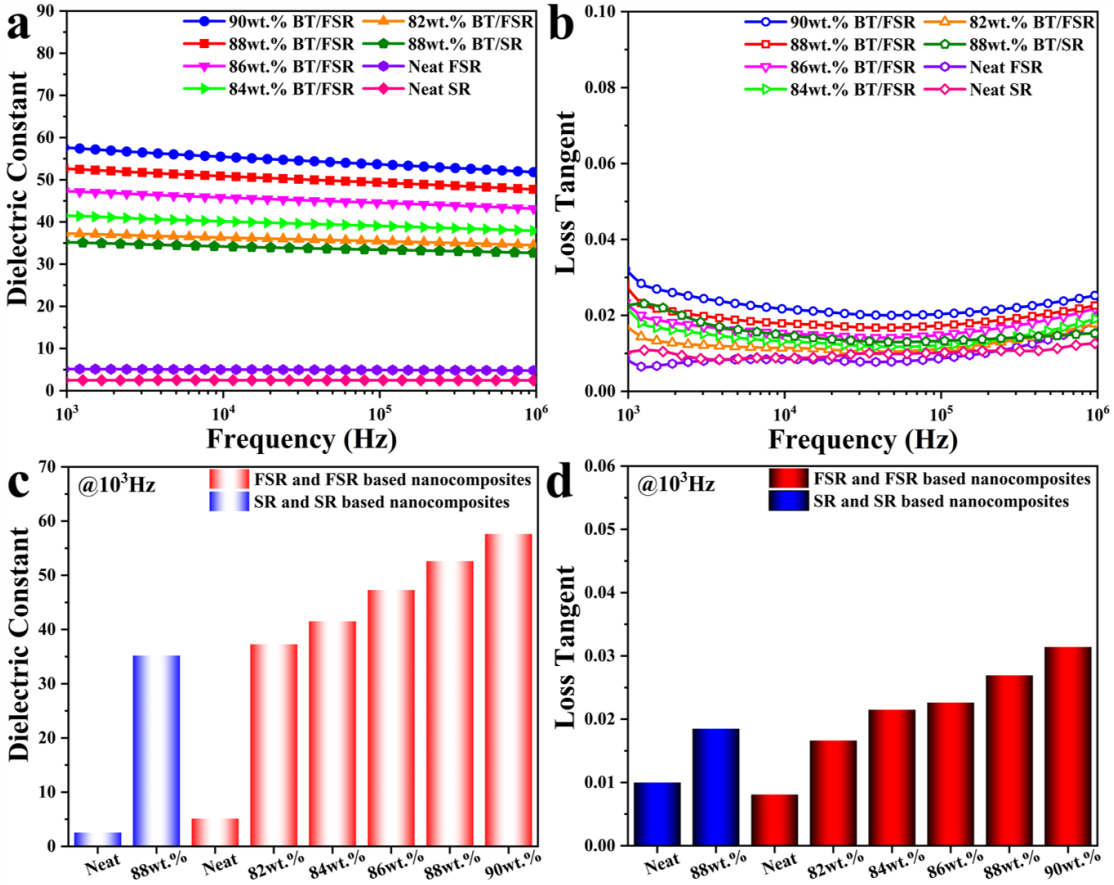

Figure 6. Dielectric properties of neat polymers and its highly-filled nanocomposites

Breakdown strength is another important parameter to polymer nanocomposites for dielectric uses. It is also related to the dispersion of dielectric nanoparticles and interfacial compatibility in polymer nanocomposites. The dielectric failure probability of neat SR, neat FSR, 88 wt% BT/SR, 88 wt% BT/FSR, 82 wt% BT/SR and 82 wt% BT/FSR nanocomposites is studied according to the Weibull distribution function.

$$P(E) = 1 - e^{-(E/E_b)^{\beta}} \qquad (2)$$

where P(E) is the cumulative failure probability, E is the measured breakdown strength, E_b is the Weibull breakdown strength with 63.2% probability to breakdown, and b is the shape parameter or the slope of the derived logarithm equation as

$$\ln[-\ln(1-P_{(E)})] = \beta \ln E - \beta \ln E_b \qquad (3)$$

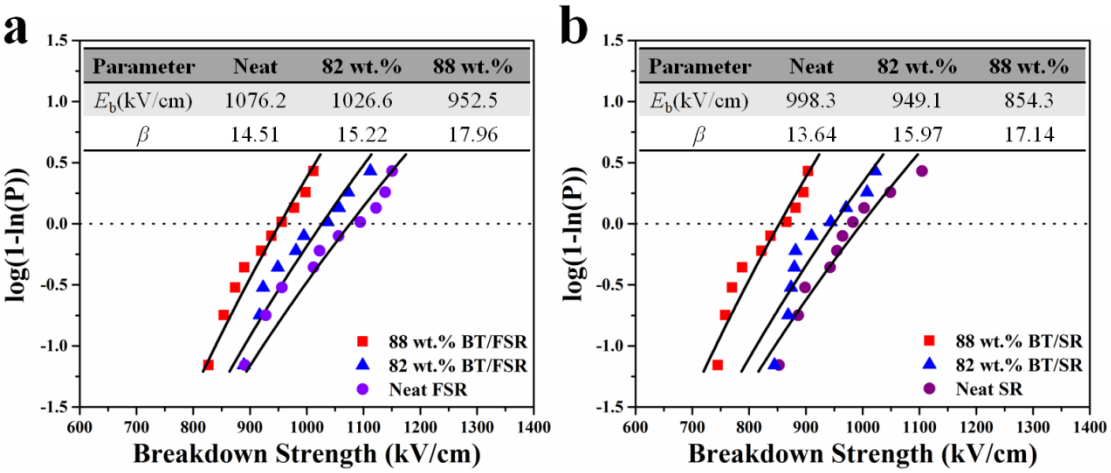

Figure 7. Cumulative failure probability of neat polymers and their highly-filled polymer nanocomposites

The linear fitted breakdown strength results of the BT/FSR and BT/SR nanocomposites are summarized in **Figure 7**. The E_b of neat SR is 998.3 kV cm^{-1}. A slight increase of the breakdown strength to 1076.2 kV cm^{-1} is obtained for the neat FSR. Furthermore, 952.5 kV cm^{-1} of breakdown strength is observed for 88 wt% BT/FSR nanocomposite, which is also higher than that of 88 wt% BT/SR nanocomposite (853.1 kV cm^{-1}). It is believed that the interfacial defects in highly filled polymer nanocomposites cause the inferior breakdown strength to that of neat polymer. Here, 82 wt% BT/FSR nanocomposite displays 1026.6 kV cm^{-1} of breakdown strength that is very close to that of the neat FSR. It implies that fewer interfacial defects exist in the 82 wt% BT/FSR nanocomposite. Besides, the β value increases from 15.06 for 82 wt% BT/FSR nanocomposite, to 16.57 for the 88 wt% BT/FSR nanocomposite, and to 17.04 for the 88 wt% BT/SR nanocomposite. The narrow distribution of breakdown strength means the highly-filled nanocomposites

exhibit superior uniformity.

The side chain in the fluorinated polysiloxane has intrinsic dipoles (C-F) that can produce strong oriented polarization under external electric field. Then it contributes to relatively high dielectric constant. However, the response speed of the dipoles cannot keep up with the alternating external electric field at high frequency, which causes deflection disorder and internal friction, as depicted in **Figure 8(a)**. Therefore, the dielectric constant of the FSR decreases and its dielectric loss increases as increasing the frequency. For the orientation polarization of dipoles, the occurring frequency of obvious relaxation is positively related to the regularity of the environment around the dipole. Polar polymers are different from highly ordered ferroelectric ceramic, which are in short-range ordered. Dipoles within polymers such as chain segments and side chains tend to be hindered by other chain segments or side chains when they respond to the external electric field [13, 47-48]. Thus, obvious relaxation of the dipole can be found at lower frequency, which causes a significant increase of dielectric loss.

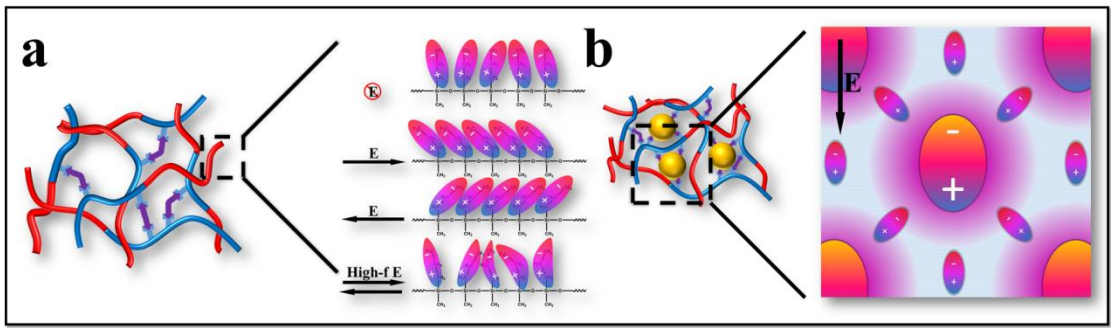

Figure 8. Schematic of dipole polarization in polar polymer (a) and its nanocomposites (b) under external electric field

Figure 8(b) depicts the schematic for the internal interaction of polar polymers and dielectric nanoparticles in highly-filled polar polymer nanocomposites under external electric field. Two kinds of dipoles within polar polymer and dielectric nanoparticles can be oriented under external electric field and their intrinsic polarizations tend to be presented at the same time. Classically theoretical models have been proposed to predict the dielectric constant of polymer nanocomposites, as

depicted in **Table S2**. According to the EMT model, good conformity had been found for highly filled BT/SR nanocomposites [40]. However, it can be seen that the experiment dielectric constant of highly filled BT/FSR nanocomposites fails to well match with the EMT model. Instead, the J-S theoretical model can describe the trend of the dielectric constant for the nanocomposites, as depicted in **Figure S3**. The reason is probably that EMT model is related to the filler loading and the morphology of composites while J-S model is related to the interactions between particles [49]. For the polar polymer matrix, this relationship is more applicable to the interaction between polar polymer matrix and dielectric nanoparticles under external electric field. So J-S model seems suitable for the BT/FSR nanocomposites. Despite that, polar polymer nanocomposites display higher dielectric constant than non-polar polymer nanocomposites due to the additional polarization from the polar polymer matrix. Therefore, integrating fluorinated silicone rubber and high loading BT nanoparticles can make the best of their intrinsic polarizations for greatly enhanced dielectric constant of polymer nanocomposites.

Conclusion

In this work, high loading BT nanoparticles are chemically bonded with fluorinated silicone rubber via thiol-ene click technique, leading to uniform dispersion of nanoparticles and good interfacial compatibility in highly filled polar polymer nanocomposites. In addition, desirable morphologies promote exploiting the polarizations of fluorinated silicone rubber and BT nanoparticles. 88 wt.% BT/FSR nanocomposite shows about 1.45 times higher dielectric constant at 10^3 Hz and 80 kV/cm higher breakdown strength than that of 88 wt.% BT/SR nanocomposite. Meanwhile, the dielectric loss of BT/FSR nanocomposite gradually decreases from 90 to 82 wt.% BT loading and the lowest value is comparable to neat polymer. This work provides an effective strategy to explore the integrated properties of highly-filled polymer nanocomposites.

Experimental section

Materials: $BaTiO_3$ (BT) nanoparticles (HBT-010, $\bar{d}$ ≈100 nm, tetragonal crystal) were supplied by Shandong Sinocera Functional Material Company. (3-Mercaptopropyl) triethoxysilane (KH580), tetramethylammonium hydroxide (TMAH), 3, 6-Dioxa-1, 8-octanedithioln, and 2, 2-Dimethoxy-2-phenylacetophenone (DMPA) were purchased from Shanghai Aladdin Bio-Chem Technology Co., LTD. 1,3,5,7-tetravinyl-1,3,5,7-tetramethylcyclotetrasiloxane (V_4) and 1,3,5-Trimethyl-1,3,5-tris(3,3,3-trifluoropropyl)cyclotrisiloxane (D_3F) were purchased from Guangdong Weng Jiang Reagent Co., Ltd. Hydrogen peroxide solution (H_2O_2 solution, 30 wt.%), ethanol and toluene were purchased from Chengdu Ke Long Reagent Co., Ltd. All the materials were directly used without treatment.

Surface modification of BT nanoparticles: A two-step modification was used for surface treatment of nanoparticles. First, a mixture with nanoparticles and H_2O_2 solution was first ultrasonically treated for 30 minutes and then heated at 105 °C for 9h under intense stirring with reflux. After that, the mixture was centrifuged for washing with deionized water and ethanol repeatedly, and dried under vacuum in sequence. Second, the dried product was added into toluene and ultrasonically treated again. Then, KH580 was introduced into the mixture and stirred at 30 °C under N_2 atmosphere for 48h. After that, the mixture was centrifuged for washing with toluene repeatedly and dried under vacuum at room temperature in sequence. Finally, sulfhydrylated $BaTiO_3$ nanoparticles (BT-SH) were obtained.

Synthesis of fluorinated polysiloxane: V_4 and D_3F (with a volume ratio of 4:6) as the monomers and TMAH as the initiator were applied to synthesize Poly(methylvinylsiloxane-methyltrifluoropropylsiloxane) via anionic ring opening polymerization. For comparison, Polymethylvinylsiloxane is also prepared according to the same preparation method of fluorinated polysiloxane with V_4 as monomer.

Preparation of $BaTiO_3$/ fluorinated silicone rubber (BT/FSR) nanocomposites: Functional nanoparticles (BT-SH), fluorinated polysiloxane, cross-linker, and initiator were mixed with toluene under intense stirring. The toluene was removed under vacuum at room temperature. Then the powder was put into a mold and initially pressed at 1.0 MPa for 1 minute. After that, the pill was isostatically pressed at 260 MPa for 10 mins. Finally, the pressed pill was treated under vacuum at 80°C for 24h and the BT/FSR nanocomposites were obtained. For comparison, $BaTiO_3$/silicone rubber (BT/SR) nanocomposites were prepared completely according to the same preparation method, which is used to highlight the roles of the fluoropolymer in the dielectric properties of highly-filled polymer nanocomposites. The measured density of the nanocomposites filled with 88 wt % BT is about 5.38 g/cm^3.

Structure characterization and performance evaluation: Fourier transform infrared spectrometer (FT-IR, IS50, Nicolet, USA) and superconducting nuclear magnetic resonance spectrometer (NMR, AVANCE 111600MHZ, Bruker, Swiss) were applied to characterize the structure of the prepared polysiloxanes. The scanning electron microscope (SEM, JSM-7610F, JEOL, Japan) and the transmission electron microscope (TEM, Libra200, Carl Zeiss, Germany) were applied to examine the morphologies of the polymer nanocomposites. The TEM-EDX was used to characterize the elemental composition and distribution in the nanocomposites. The samples were sputtered with 8 mm diameter gold electrode on both sides. The dielectric properties were evaluated using Precision Impedance Analyzer (4294A, Agilent Technologies Inc., USA) at a range from 10^3 Hz to 10^7 Hz. Shore D hardness test was applied to evaluate effects of high loading BT nanoparticles on the hardness of polymer nanocomposites.

Conflicts of interest

The authors declare no conflicts of interest.

Acknowledgements

This work was supported by the National Natural Science Foundation of China (11747042) and Project of State Key Laboratory of Environment-friendly Energy Materials (19FKSY0102).

References

1 Q. Li, L. Chen, M. R. Gadinski, S. Zhang, G. Zhang, H. Li, A. Haque, L. Q. Chen, T. Jackson and Q. Wang, *Nature*, 2015, **523**, 576-580.

2 Prateek, V. K. Thakur, and R. K. Gupta, *Chem. Rev.*, 2016, **116**, 4260-4317.

3 H. Luo, X. Zhou, C. Ellingford, Y. Zhang, S. Chen, K. Zhou, D. Zhang, C. R. Bowen and C. Wan, *Chem. Soc. Rev.*, 2019, **48**, 4424-4465.

4 B. Fan, M. Zhou, C. Zhang, D. Hea and J. Bai, *Prog. Polym. Sci.*, 2019, **97**, 101143.

5 T. M. Linker, S. Tiwari, H. Kumazoe, S. Fukushima, R. K. Kalia, A. Nakano, R. Ramprasad, F. Shimojo, and P. Vashisht, *J. Phys. Chem. Lett.*, 2020, **11**, 352-358.

6 J. Che, W. Neri, I. Ly, P. Poulin, C. Zakri, J. Yuan, *ACS Appl. Energy Mater.*, 2020, **3**, 9107-9116.

7 D. Q. Tan, *Adv. Funct. Mater.*, 2020, **30**, 1808567.

8 D. Jiang, Z. Fan, H. Wang, M.i Xu, G. Chen, Y. Song, and Z. L. Wang, *ACS Nano* 2020, **14**, 15394-15402.

9 Q. Wang, H. Ding, X. Hu, X. Liang, M. Wang, Q. Liu, Z. Li and G. Sun, *Mater. Horiz.*, 2020, **7**, 2673-2682.

10 J. Zhang, Z. Yan, X. Liu, Y. Zhang, H. Zou, Y. Le, and J.-F. Chen, *ACS Appl. Mater. Interfaces*, 2020, **12**, 53076-53087.

11 F. Hu, L. An, A. T. Chivate, Z. Guo, S. V. Khuje, Y. Huang, Y. Hu, J. Armstrong, C. Zhou and S. Ren, *Chem. Commun.*, 2020, **56**, 2332-2335.

12 Y. Zhou, Q. Wang, *J. Appl. Phys.*, 2020, **127**, 240902.

13 J. Wei, L. Zhu, *Prog. Polym. Sci.*, 2020, **106**, 101254

14 L. Zhu, and Q. Wang, *Macromolecules*, 2012, **45**, 2937-2954.

15 P. Mao, J. Wang, L. Zhang, Q. Sun, X. Liu, L. He, S. Liu, S. Zhang and H. Gong, *Phys. Chem. Chem. Phys.*, 2020, **22**, 13143-13153

16 Y. Jiang, M. Zhou, Z. Shen, X. Zhang, H. Pan and Y.-H.a Lin, *APL Materials*, 2021, **9**, 020905.

17 M. Yuan, B. Li, S. Zhang, R. Rajagopalan, and M. T. Lanagan, *ACS Appl. Polym. Mater.*, 2020, **2**, 1356-1368.

18 X. Liang, X. Yu, L. Lv, T. Zhao, S. Luo, S. Yu, R. Sun, C.-P. Wong, P. Zhu, *Nano Energy*, 2020, **68**, 104351.

19 R. Guo, J. I. Roscow, C. R. Bowen, H. Luo, Y. Huang, Y. Ma, K. Zhou and D. Zhang, *J. Mater. Chem. A*, 2020, **8**, 3135-3144.

20 M. A. Marwat, W. Ma, P. Fan, H. Elahi, C. Samart, B. Nan, H. Tan, D. Salamon, B. Ye, H. Zhang, *Energy Storage Mater.*, 2020, **31**, 492-504.

21 M. M. Rueda, M.-C. Auscher, R. Fulchiron, T. Perie, G. Martin, P. Sonntag, P. Cassagnau, *Prog. Polym. Sci.*, 2017, **66**, 22-53.

22 Y. Song, Q. Zheng, *Prog. Mater. Sci.*, 2016, **84**, 1-58.

23 Y. Feng, Q. Deng, C. Peng, J. Hu, Y. Li, Q. Wu, Z. Xu, *J. Mater. Chem. C.*, 2018, **6**, 13283-13292.

24 P. Kim, N. M. Doss, J. P. Tillotson, P. J. Hotchkiss, M.-J. Pan, S. R. Marder, J. Li, J. P. Calame, J. W. Perry, *ACS Nano.*, 2009, **3**, 2581-2592.

25 T. J. Lewis, *IEEE Trans. Dielectr. Electr. Insul.*, 2004, **11**, 739-753.

26 O. Levy and D. Stroud, *Phys. Rev. B: Condens. Matter Mater. Phys.*, 1997, **56**, 8035.

27 E. Baer and L. Zhu, *Macromolecules*, 2017, **50**, 2239-2256.

28 Z. Pan, L. Yao, J. Zhai, X. Yao and H. Chen, *Adv. Mater.*, 2018, **30**, 1705662.

29 J. Liu, Y. Zhang, Z. Wang, J. Ding, S. Yu, Y. Zhang and Z. Jiang, *Nanoscale*, 2020, **12**, 12416-12425.

30 X. Huang, B. Sun, Y. Zhu, S. Li, P. Jiang, *Prog. Mater. Sci.*, 2019, **100**, 187-225.

31 J. I. Roscow, C. R. Bowen, D. P. Almond, *ACS Energy Lett.*, 2017, **2**, 2264-2269.

32 S. Liu, B. Shen, H. Hao and J. Zhai, *J. Mater. Chem. C*, 2019, **7**, 15118-15135.

33 Y. Li, Y. Zhou, Y. Zhu, S. Cheng, C. Yuan, J. Hu, J. He and Q. Li, *J. Mater. Chem. A*, 2020, **8**, 6576-6585.

34 P.-J. Wang, D. Zhou, H.-H. Guo, W.-F. Liu, J.-Z. Su, M.-S. Fu, C. Singh, S. Trukhanovfgh and A. Trukhanov, *J. Mater. Chem. A*, 2020, **8**, 11124-11132.

35 H. Hu, F. Zhang, S. Luo, W. Chang, J. Yue, C.-H. Wang, *Nano Energy*, 2020, **74**, 104844.

36 J. Liu, Z. Shen, W. Xu, Y. Zhang, X. Qian, Z. Jiang and Y. Zhang, *Small*, 2020, **16**, 2000714.

37 H. Ye, X. Zhang, C. Xu, B. Han and L. Xu, *J. Mater. Chem. C*, 2018, **6**, 11144-11155.

38 K. Yang, X. Huang, M. Zhu, L. Xie, T. Tanaka and P. Jiang, *ACS Appl. Mater. Interfaces*, 2014, **6**, 1812-1822.

39 Y. Kim, M. Kathaperumal, V. W. Chen, Y. Park, C. FuentesHernandez, M.-J. Pan, B. Kippelen and J. W. Perry, *Adv. Energy Mater.*, 2015, **5**, 1500767.

40 R.-C. Chen, Q.-P. Zhang, K. Ke, N. Sun, W.i-D. Xu, D. Liu, Y.-T. Li, W. Yang, Y. Zhou, M.-B. Yang, J. Yuan, W. Yang, *J. Mater. Chem. C*, 2020, **8**, 8786-8795.

41 B. F. Ezzahra, M. Raihane, and B. Ameduri, *Prog. Mater. Sci.*, 2020, **113**, 100670.

42 J. H. L. Ngai, C. C. M. Chan, C. H. Y. Ho, J. K. W. Ho, S. H. Cheung, H. Yin and S. K. So, *Mater. Adv.*, 2020, **1**, 891-898.

43 Y. Yang, Y. Zhao, J. Liu, Z. Nie, J. Ma, M. Hua, Y. Zhang, X. Cai and X. He, *ACS Materials Lett.*, 2020, **2**, 453-460.

44 S. Sami, R. Alessandri, R. Broer, R. W. A. Havenith, *ACS Appl. Mater. Interfaces*, 2020, **12**, 17783-17789.

45 Q.-P. Zhang, J.-H. Liu, H.-D. Liu, F. Jia, Y.-L. Zhou, J. Zheng, *Appl. Phys. Lett.*, 2017, **111**, 152901.

46 L. G. Bach, M. R. Islam, J. T. Kim, S. Y. Seo and K. T. Lim, *Appl. Surf. Sci.*, 2012, **258**, 2959-2966.

47 J. Mijovic, J. W. Sy, T. K. Kwei, *Macromolecules*, 1997, **30**, 3042-3050.

48 K. Qian, R. Qiao, S. Chen, H. Luo and D. Zhang, *J. Mater. Chem. C*, 2020, **8**, 8440-8450.

49 S. Luo, Y. Shen, S. Yu, Y. Wan, W.-H. Liao, R. Sun and C.-P. Wong, *Energy Environ. Sci.*, 2017, **10**, 137-144.